PNAS RESEARCH ARTICLE | BIOCHEMISTRY

A widespread family of ribosomal peptide metallophores involved in bacterial adaptation to metal stress

Laura Leprevost[a,1], Sophie Jünger[b,1], Guy Lippens[c,2], Céline Guillaume[b], Giuseppe Sicoli[d], Lydie Oliveira[e], Enrico Falcone[f], Emiliano de Santis[g], Alex Rivera-Millot[a,3], Gabriel Billon[d], Francesco Stellato[g], Céline Henry[e], Rudy Antoine[a,2], Séverine Zirah[b,2], Svetlana Dubiley[c,2,4], Yanyan Li[b,2,4], and Françoise Jacob-Dubuisson[a,2,4]

Affiliations are included on p. 10.

Edited by Wilfred van der Donk, University of Illinois at Urbana-Champaign, Urbana, IL; received May 13, 2024; accepted October 15, 2024

Ribosomally synthesized and posttranslationally modified peptides (RiPPs) are a structurally diverse group of natural products that bacteria employ in their survival strategies. Herein, we characterized the structure, the biosynthetic pathway, and the mode of action of a RiPP family called bufferins. With thousands of homologous biosynthetic gene clusters throughout the bacterial phylogenetic tree, bufferins form by far the largest family of RiPPs modified by multinuclear nonheme iron-dependent oxidases (MNIO, DUF692 family). Using *Caulobacter vibrioides* bufferins as a model, we showed that the conserved Cys residues of their precursors are transformed into 5-thiooxazoles, further expanding the reaction range of MNIO enzymes. This rare modification is installed in conjunction with a partner protein of the DUF2063 family. Bufferin precursors are rare examples of bacterial RiPPs found to feature an N-terminal Sec signal peptide allowing them to be exported by the ubiquitous Sec pathway. We reveal that bufferins are involved in copper homeostasis, and their metal-binding propensity requires the thiooxazole heterocycles. Bufferins enhance bacterial growth under copper stress by complexing excess metal ions. Our study thus describes a large family of RiPP metallophores and unveils a widespread but overlooked metal homeostasis mechanism in bacteria.

ribosomally synthesized and post-translationally modified peptide (RiPP) | metallophore | multinuclear non-heme iron-dependent oxidase (MNIO)

Ribosomally synthesized and posttranslationally modified peptides (RiPPs) are natural products with a tremendous variety of structures and biological activities (1–3). They are synthesized from a gene-encoded precursor peptide, generally composed of an N-terminal leader sequence and a core sequence where posttranslational modifications (PTMs) occur. In many cases, a pathway-specific RiPP recognition element (RRE) domain interacts with the leader sequence and mediates recruitment of the modification enzymes (4–6). RRE domains are thus a hallmark of RiPP biosynthesis. The vast structural diversity of RiPPs is conferred by virtually unlimited possibilities of chemical transformations. An emerging family of PTM enzymes is the DUF692 family of multinuclear nonheme iron-dependent oxidases (MNIOs) that catalyze various reactions in the biosynthesis of diverse RiPPs, mostly but not exclusively on Cys residues (7–13). These reactions include oxazolone coupled to thioamide formation, excision of cysteine β-methylene, Cys-involved macrocyclization, and C–C and C–N cleavages (7, 8, 11–13). However, the full spectrum of MNIO activities remains far from being fully appreciated.

Four-gene *gig* operons (*gig* for gold-induced genes) encoding DUF692 (MNIO) family proteins were identified in the genomes of several microbial species (*SI Appendix*, Fig. S1). In *Cupriavidus metallidurans* (RMET_RS24090-RS24075), *Legionella pneumophila* (LPG_RS10595-LPG_RS10580), and *Caulobacter vibrioides* (CCNA_03363-CCNA_03366), the expression of these operons is induced under various transition metal stresses that include gold, cadmium, copper, etc., whereas in *Bordetella pertussis* (BP_RS14685-BP_RS14700), it is controlled by the master regulator of virulence BvgAS (14–18). Orthologous operons were notably found in methane-oxidizing bacteria (19). However, despite genetic evidence for an involvement in the copper-resistant phenotype in *C. metallidurans* (20), the function of these operons remains elusive. Based on their composition, we speculated that they are biosynthetic gene clusters (BGCs) whose products could represent a previously unknown RiPP family. Unlike most previously described RiPPs however, these putative precursors have predicted Sec signal peptides. Using genetic, structural, and bioinformatic analyses, we questioned the function, the mode of action, and the prevalence of *gig*-like operons in bacteria.

Significance

Copper is both essential and toxic in excess. Bacteria face copper in their environments, notably in phagocytes, hence they have developed several defense mechanisms. We found a strategy of protection from copper, through the biosynthesis of natural products that we named bufferins. Bufferins are ribosomally synthesized posttranslationally modified peptides (RiPPs), natural products with key roles in bacterial physiology and ecology. Model bufferins enhance bacterial growth under copper stress by complexing with the metal using thiooxazole heterocycles that result from enzymatic modification of cysteine residues. With thousands of homologs throughout the bacterial phylogenetic tree, bufferins represent a highly prevalent strategy for maintaining the homeostasis of copper, and possibly of other metals.

Preprint server: This article was deposited as a preprint in BioRxiv (bioRxiv 2024.03.18.585515).

The authors declare no competing interest.

This article is a PNAS Direct Submission.

[1]L.L. and S.J. contributed equally to this work.

[2]G.L., R.A., S.Z., S.D., Y.L., and F.J.-D. contributed equally to this work.

[3]Present address: Institut National de la Recherche Scientifique-Centre Armand-Frappier Santé Biotechnologie, Bacterial Symbionts Evolution, Laval, QC H7V 1B7, Canada.

[4]To whom correspondence may be addressed. Email: svetlana.dubiley@gmail.com, yanyanli@mnhn.fr, or francoise.jacob@ibl.cnrs.fr.

This article contains supporting information online at https://www.pnas.org/lookup/suppl/doi:10.1073/pnas.2408304121/-/DCSupplemental.

Published November 27, 2024.

We report the characterization of the products of the *C. vibrioides gig*-like BGCs, the first representatives of bufferins, a unique family of RiPPs. We revealed that bufferins are small protein metallophores containing rare 5-thiooxazole modifications of Cys residues. The joint action of the DUF692 (MNIO) and DUF2063 proteins is required to install this posttranslational modification. We showed that the *C. vibrioides* bufferins protect bacteria against toxic concentrations of copper by binding the excess metal in the periplasm. Our bioinformatic study suggests that bufferins likely represent an overlooked copper defense mechanism very common in Hydrobacteria and Terrabacteria.

Results

Large RiPP Family Involving MNIOs. We performed an in silico analysis of the CCNA_03363-03366 operon of *C. vibrioides*, hereafter named *buf1*, to gain insight into gene functions. CCNA_03363 encodes a DUF2282-family protein (BufA1), whose members are 80 to 120 residues long and harbor four Cys residues (Cys^{I} to Cys^{IV}) and a predicted Sec signal peptide (Fig. 1*A*). We hypothesized that BufA1 is an unusually long precursor peptide whose translocation across the cytoplasmic membrane would rely on the ubiquitous Sec export pathway rather than on a specialized export system as is often the case for secreted

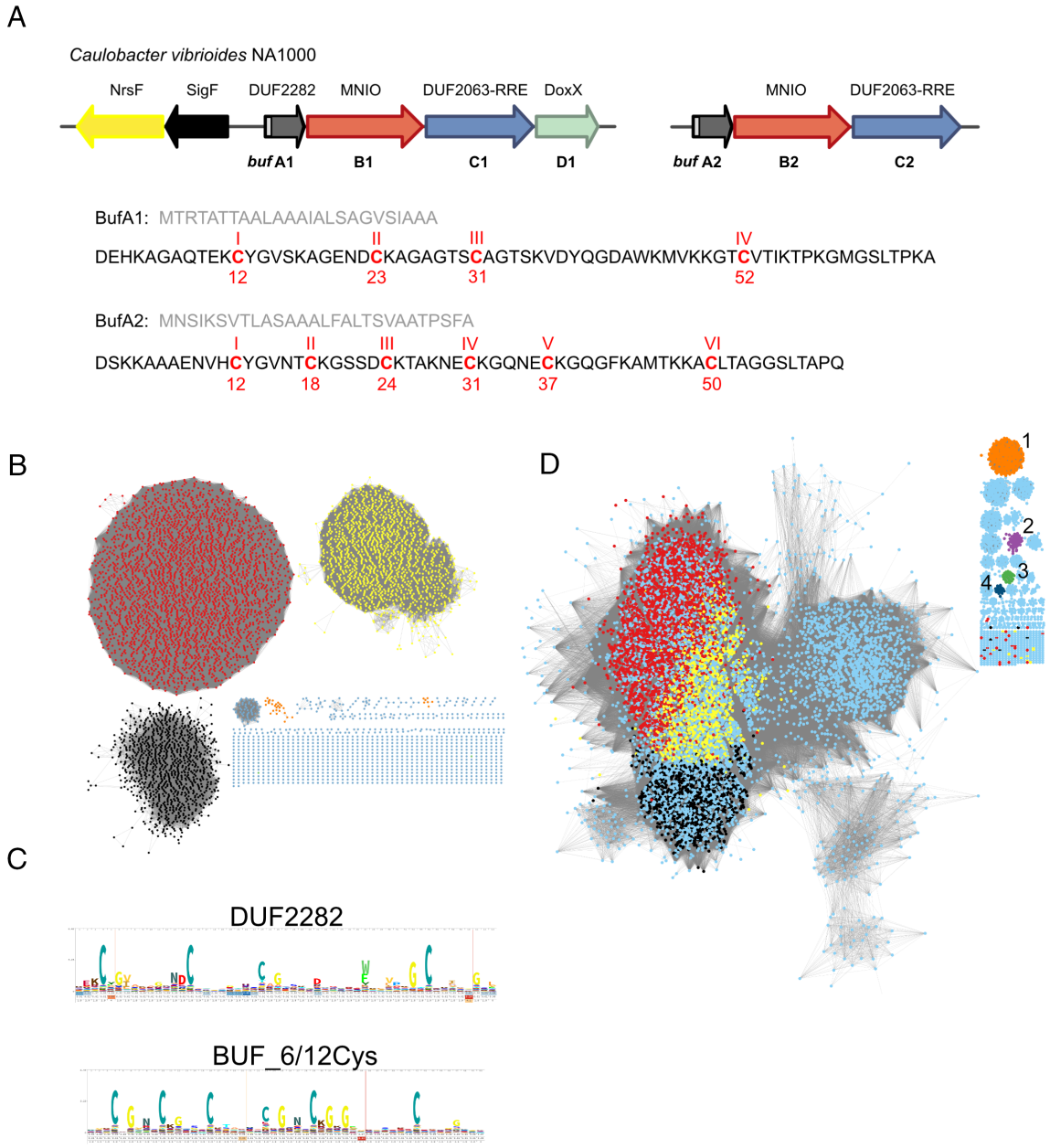

Fig. 1. In silico analyses of the bufferin family. (*A*) Gene composition of the *buf1* and *buf2* BGCs and sequences of BufA1 and BufA2 with the Cys residues labeled (numbering according to the core peptides). The signal peptide and core peptide sequences are in pale and dark gray, respectively. In the vicinity of *buf1ABCD* are genes coding for SigF and the anti-sigma factor NrsF that regulate *buf1* and *buf2* expression. (*B*) SSN analysis of bufferin-like precursors genetically associated with MNIOs. DUF2282 and BUF_6/12Cys proteins, including BufA1 and BufA2 of *C. vibrioides*, belong to the largest two clusters (red and yellow dots), respectively. The oxazolins are shown as black dots. Small clusters in orange contain chryseobasins (7) that are predicted to harbor signal peptides. (*C*) Weblogos for the DUF2282 and BUF_6/12Cys bufferins. (*D*) SSN analysis of MNIOs (at 80% identity). MNIOs genetically associated with DUF2282 and BUF_6/12Cys proteins, including BufB1 and BufB2 of *C. vibrioides*, are in red and yellow, respectively. Those associated with oxazolins are colored black. MNIOs associated with chryseobasins, methanobactins, TglA-type pearlins, and aminopyruvatides are found in small clusters numbered 1 to 4.

RiPPs (21). The AlphaFold2 model predicts that the 68-residue long BufA1 peptide—after removal of the predicted Sec signal peptide—contains a 2-stranded β sheet, some α-helical structure, and a disulfide (S–S) bond between the first β strand and the short α helix (*SI Appendix*, Fig. S1). Mature BufA1 is predicted with good confidence to fold as a small protein rather than being a totally unstructured peptide (*SI Appendix*, Figs. S1 and S2).

The product of CCNA_03364 (BufB1) belongs to the MNIO family, whereas CCNA_03365 codes for a protein (BufC1) with an uncharacterized N-terminal DUF2063 domain. The predicted structural model of BufC1 revealed that its C-terminal domain is related to RRE domains (4–6) (*SI Appendix*, Fig. S1). In light of recent discoveries of MNIOs involved in RiPP biosynthesis (7–13), we hypothesized that BufB1 and BufC1 would install modifications on Cys residues of BufA1. Finally, CCNA_03366 encodes a putative DoxX-type oxido-reductase, BufD1 (22, 23).

Inspection of the *C. vibrioides* genome identified a second operon, the *buf2* BGC (CCNA_02999-03001) (Fig. 1*A*) which encodes homologs of BufB1 (CCNA_03000) and BufC1 (CCNA_02999) but lacks a *bufD1*-like gene. Like BufA1, its putative precursor peptide BufA2 (CCNA_03001) possesses a predicted Sec signal peptide. Its 61-residue core peptide contains six Cys residues (Cys^{I} to Cys^{VI}) (Fig. 1*A*). Although its predicted 3D structure is very similar to that of BufA1 (*SI Appendix*, Figs. S1 and S2), this small protein does not have a corresponding profile in the databases of protein families.

To evaluate the abundance of homologous BGCs, we collected >14,000 MNIO protein sequences from the NCBI nonredundant database. The retrieved sequences are widely distributed throughout Pseudomonadota, Terrabacteria, Myxococcota, Fibrobacteres/Chlorobi/Bacterioidetes, Planctomycetes/Verrucomicrobia/*Chlamydia*, and Acidobacteriota. We analyzed their genomic contexts and collected associated genes coding for putative bufferin-like precursors, i.e., small proteins with Cys residues and a predicted Sec signal peptide. Thousands of these were collected, some of which are markedly larger than typical RiPP precursors and harbor numerous Cys residues (detailed in silico analyses will be published separately). Notably, the recently described MNIO-modified oxazolins were identified in this search (24).

In a sequence similarity network (SSN) constructed with these proteins, the largest cluster corresponds to the DUF2282 signature, including *C. vibrioides* BufA1 (Fig. 1*B*). BufA2 of *C. vibrioides* belongs to the second-largest cluster of proteins characterized by six or 12 conserved Cys residues, which we named BUF_6/12Cys (Fig. 1 *B* and *C*). Of note, BUF_6/12Cys proteins were previously identified in Antarctic soil metagenomes (25). The oxazolins were found to belong to a different cluster than DUF2282 or BUF_6/12Cys bufferins. Parallel SSN analyses of the MNIO superfamily (Fig. 1*D*) showed that those coded in the DUF2282 and BUF_6/12Cys BGCs belong to the most populated sequence cluster, distinct from small clusters of MNIOs involved in the biosynthesis of other RiPP types (7, 9–11, 13). The MNIO enzymes associated with oxazolins were found in a distinct area of the large sequence cluster (Fig. 1*D*). Together our data indicate that bufferins currently form the largest group of MNIO-associated RiPPs.

Bufferins Mediate Adaptation to Copper Stress. In *C. vibrioides*, *buf1* and *buf2* BGCs belong to the SigF-controlled, core regulon of copper stress (15, 17, 26). To test whether they could be upregulated by other biologically relevant metals, we generated reporter fusions within *bufA1* and *bufA2* and confirmed that both are induced by high concentrations of Cu^{2+}, but not by Fe^{2+}, Zn^{2+}, or Mn^{2+} (Fig. 2*A* and *SI Appendix*, Fig. S3).

To determine whether bufferins, the putative RiPP products of the *buf* BGCs, contribute to adaptation to excess copper, we prepared *C. vibrioides* deletion mutants that express a single (Cv_{buf1} and Cv_{buf2}) or neither BGC (Cv_{DKO}). Cv_{DKO} grew slower than the parental Cv_{WT} strain when $CuSO_4$ was added to the growth medium, unlike Cv_{buf1} or Cv_{buf2} (Fig. 2*B*). Thus, *C. vibrioides* bufferins enhance growth under copper stress and are functionally redundant. To confirm that a single BGC is sufficient to protect bacteria from excess copper, we performed gain-of-function experiments. Expression of *buf1ABCD* in an *Escherichia coli* laboratory strain enhanced survival of bacteria exposed to a bactericidal concentration of Cu^{2+} (Fig. 2*C*), unlike that of the unrelated pseudomycoidin operon *psmCA* used as a control (27). In reducing, microaerobic conditions, expression of the *buf1* operon also protected *E. coli* from Cu^{+} (Fig. 2*D*).

We then asked whether the bufferins would confer an advantage on *C. vibrioides* in biotic interactions. Since amoeba notably use copper against their bacterial preys (28), a predation assay was performed. We attempted to measure survival of *C. vibrioides* after ingestion by *Dictyostelium discoidum*, a well-established model organism for the study of phagocytosis. However, as these attempts were unsuccessful, we tested whether the presence of the *buf* BGCs might slow down bacterial killing by performing phagocytic plaque assays on agar plates (28). In this assay, bacteria tolerant to copper are killed more slowly by amoeba than copper-sensitive bacteria, and because amoeba have a limited phagocytic capacity, a lower rate of intracellular killing implies a lower rate of ingestion (28). The relative survival rates of Cv_{WT} and Cv_{DKO} were compared by placing amoebal suspensions onto bacterial lawns and measuring bacterial densities in the contact zones via densitometry scanning after incubation (Fig. 2*E*). Weaker bacterial densities with larger zones of complete clearance were observed for the Cc_{DKO} compared to the Cc_{WT} strain, consistent with a protective role of bufferins in this context.

Characterization of Bufferin PTMs. To identify the PTMs of bufferins, we engineered an IPTG-inducible version of SigF to control expression of their BGCs in *C. vibrioides*. The metabolic profiles of IPTG-treated Cv_{buf1}(pSigF) and Cv_{buf2}(pSigF) were analyzed by liquid chromatography coupled to mass spectrometry (LC-MS) and compared to that of Cv_{DKO}(pSigF) to reveal peptide species only present in the *buf*-expressing strains. In cell lysates of Cv_{buf1}(pSigF), a major species exhibited a mass matching that of BufA1 with the predicted Sec signal peptide cleaved off and a −10 Da mass shift (Fig. 3*A* and *SI Appendix*, Fig. S4 and Table S1), suggesting that the core peptide accumulates in the periplasm and contains posttranslational modifications of one or more residues. A second form with a −12 Da mass shift was also detected, but not systematically, as its presence varied according to storage conditions. The major product with a −10 Da mass shift is considered the mature peptide product and was named bufferin 1 (Buf1). Similarly, Cv_{buf2}(pSigF) produced a major peptide product with a −18 Da mass shift, called bufferin 2 (Buf2), and a minor species with a −20 Da mass shift (*SI Appendix*, Fig. S4 and Table S1).

To test the hypothesis that mature bufferins contain modified Cys residues and/or disulfide (S–S) bonds, we performed reduction and alkylation treatment of the peptides. Both the −10 Da and the −12 Da species were converted by this treatment into species with a mass shift of −8 Da and three or four alkyl groups for Buf1 (*SI Appendix*, Fig. S5). The conversion to a −8 Da species indicated the reduction of one and two S–S bonds for the −10 Da and −12 Da forms, respectively, with the −8 Da mass shift caused by PTM(s). The presence of three or four alkyl groups in reduced Buf1 suggests that the PTM(s) do not affect Cys residues or result in alkylation-sensitive groups. Similarly, for Buf2, both the −18 Da and the −20 Da species were converted into species with a

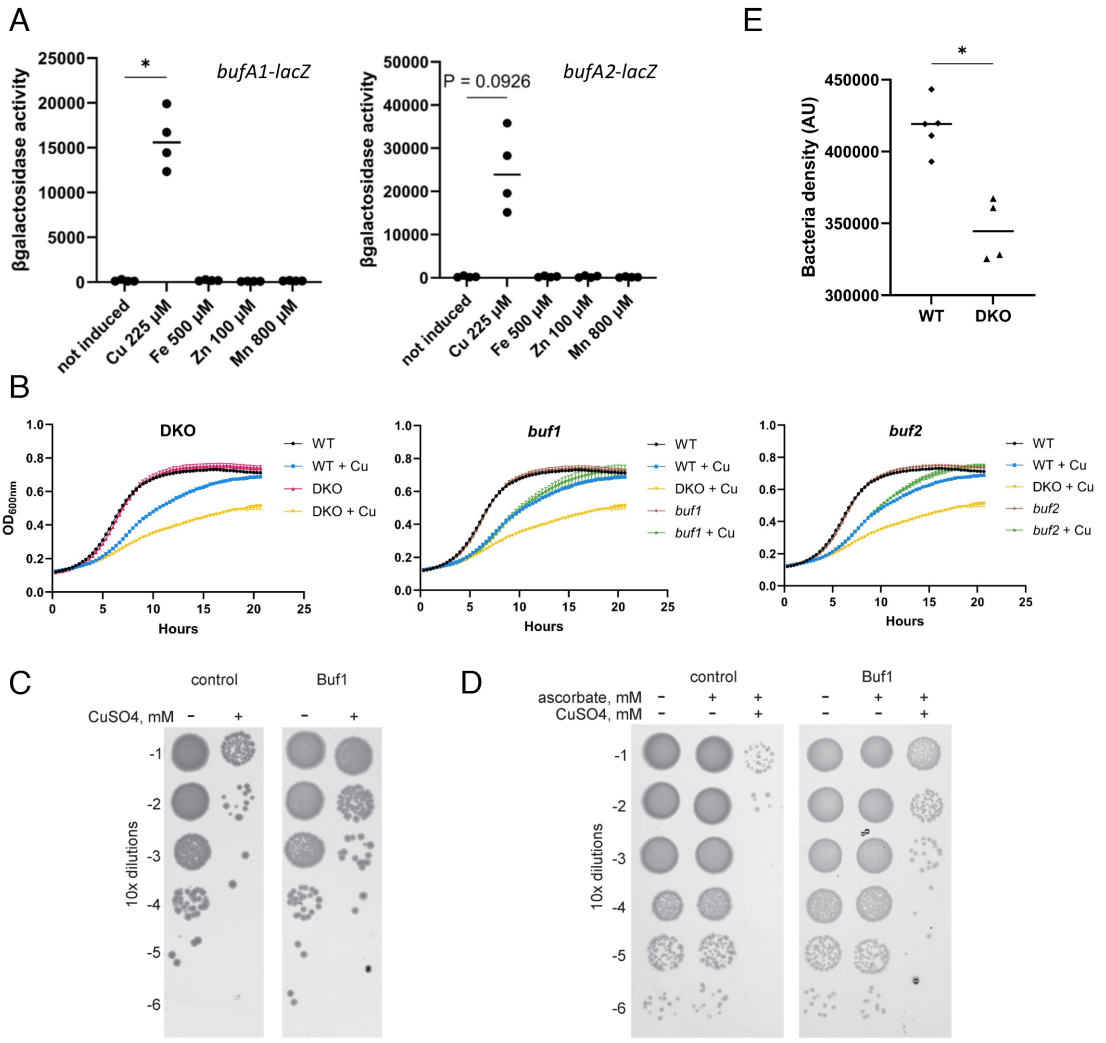

Fig. 2. Regulation and function of the bufferins. (*A*) Reporter assays with *bufA1-lacZ* and *bufA2-lacZ* transcriptional fusions. Bacteria were grown for 16 h with the indicated concentrations of $CuSO_4$, $FeSO_4$, $ZnSO_4$, or $MnCl_2$. Nonparametric, one-way ANOVA Kruskal–Wallis (two-sided) test followed by a Dunn's multiple-comparison tests were used to analyze the differences between treated cultures and the control (n = 4; * in the *Upper Left* graph indicates $P = 0.047$). (*B*) Effect of copper on bacterial growth. The Cv_{DKO}, $Cv_{buf1ABCD}$ (*buf1*), and $Cv_{buf2ABC}$ (*buf2*) strains were grown without or with 225 µM $CuSO_4$. In (*C*), expression of *buf1* in *E. coli* BL21(pCA24-buf1A^{str}BCD) grown in minimal medium was induced by IPTG, and the bacteria were challenged with 0.3 mM $CuSO_4$ for 3 h before serial dilutions. BL21(pCA24-psmCA) expressing the unrelated pseudomycoidin operon *psmCA* expressed from the same plasmid backbone was used as a control. In (*D*), expression of *buf1* in *E. coli* BL21(pCA24-buf1A^{str}BCD) grown in rich medium was induced by IPTG, followed by 2 h in microaerobic conditions with $CuSO_4$ and Cu^{2+}-reducing ascorbate as indicated, before serial dilutions. The control was as in (*C*). (*E*) Assay of bacterial lysis by *D. discoidum*. Bacterial densities in the zones of contact were determined using ImageJ analyses. A nonparametric Mann–Whitney test (two-sided) was used to analyze the differences between the Cv_{WT} strain (n = 5) and the Cv_{DKO} strain (n = 4; * indicates $P = 0.0159$). The medians are shown.

mass shift of −16 Da and four, five, or six alkyl groups (*SI Appendix*, Fig. S6). MS analyses of trypsin-digested, alkylated Buf1 revealed that Cys^{I} (Cys12) and Cys^{IV} (Cys52) (numbering according to the core peptide, see Fig. 1) had mass increments corresponding to alkylation only, indicative of unmodified residues (*SI Appendix*, Fig. S7). By contrast, in the central tryptic peptide containing Cys^{II} (Cys23) and Cys^{III} (Cys31), both Cys residues carry mass increments corresponding to alkylation with additional −4.03 Da mass shifts (Fig. 3*B*), as proposed by the untargeted PTM search solution SpecGlobX (29).

To confirm that Cys residues are required for Buf1 function, we constructed strains with the four conserved Cys residues replaced with Ser, separately or in combinations. Consistent with the proposed modifications of Cys^{II} and Cys^{III} and the presence of an S–S bond between Cys^{I} and Cys^{IV}, the substitution of either of Cys^{II} or Cys^{III} yielded peptides with mass shifts of −6 Da relative to the calculated mass of the mutated peptide (*SI Appendix*, Fig. S8). We tested the ability of the mutated BufA1 to protect *C. vibrioides* from excess copper. All mutant strains grew slower than the parental Cv_{buf1} in the presence of $CuSO_4$ (*SI Appendix*, Fig. S9), indicating the importance of both modified and unmodified Cys residues for function. However, the Buf1$^{CysISer+CysIVSer}$ variant was not detected in cell extracts by MS, suggesting that it was proteolyzed intracellularly. Altogether, the data are consistent with the presence of an S–S bond between Cys^{I} and Cys^{IV} that stabilizes the tertiary structure of the bufferin, and Cys^{II} and Cys^{III} being targets of 4-electron oxidation reactions that generate alkylation-sensitive, presumably thiol-containing groups. The Buf1 congener product with a −12 Da mass shift could correspond to a form with a labile S–S bond between the modified residues. Similarly, in Buf2, in addition to the unmodified Cys^{I} (Cys24) and Cys^{VI} (Cys50) likely forming an S–S bond (*SI Appendix*, Fig. S1), the central Cys residues carry −4.03 Da shifts (*SI Appendix*, Fig. S10).

To facilitate bufferin purification and characterization, we added C-terminal tags to BufA1 and BufA2 (*SI Appendix*, Table S1). Affinity-purified Buf1 from *C. vibrioides* cellular lysates was fully

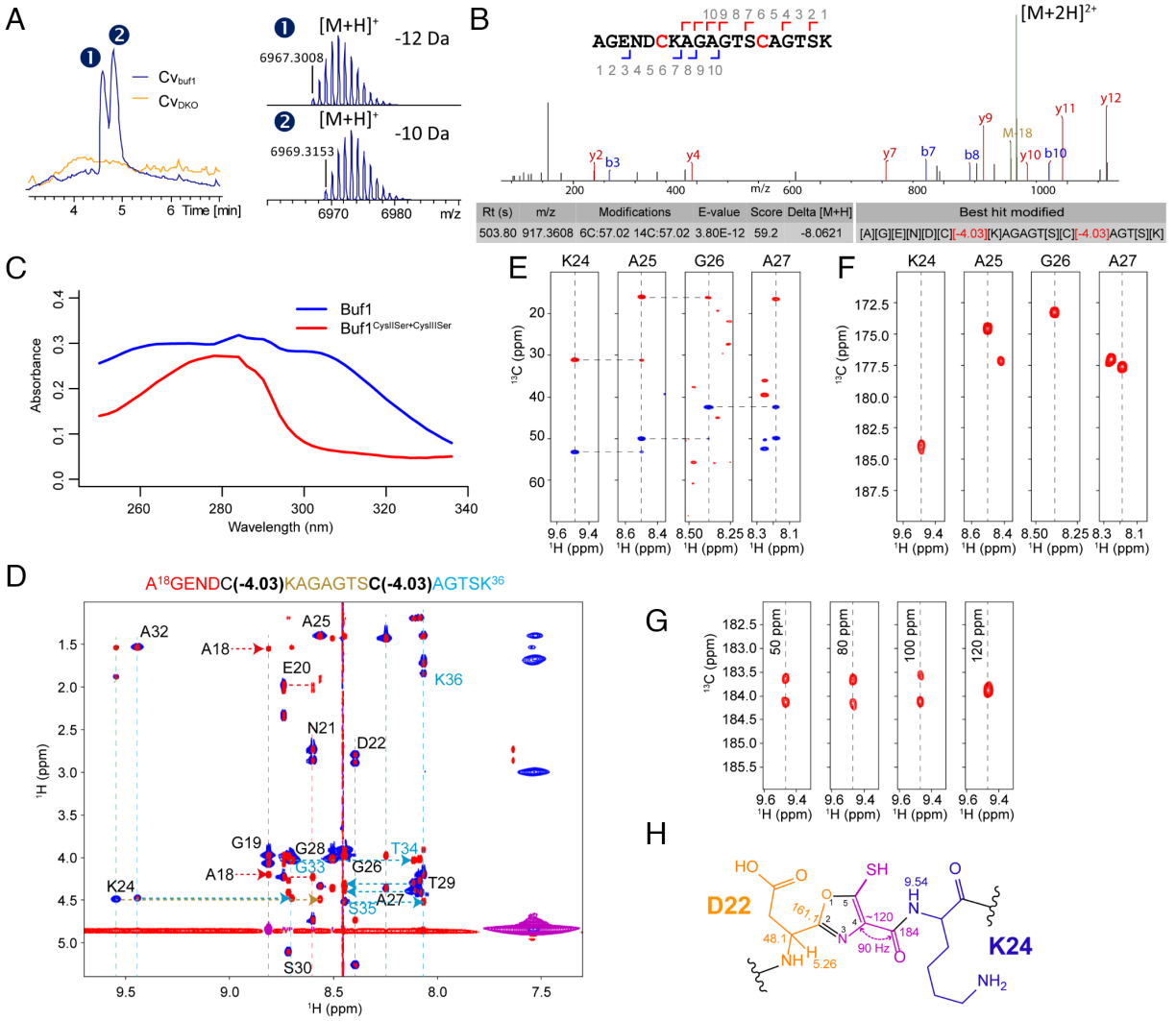

Fig. 3. Posttranslational modifications of bufferin 1. (*A*) Top–down LC-MS analyses of cell extracts of Cv$_{buf1}$(pSigF) compared with Cv$_{DKO}$(pSigF). *Left* panel: total ion chromatograms, *Right* panels: deconvoluted mass spectra of the compounds detected for Cv$_{buf1}$(pSigF). Their Mw corresponds to the core peptide (i.e., without signal peptide; calculated monoisotopic Mw = 6,978.35 Da), with mass shifts of −10 Da ([M+H]$^+$ at *m/z* 6,969.32) and −12 Da ([M+H]$^+$ at *m/z* 6,967.30). (*B*) Bottom–up analysis of Buf1. MS/MS spectrum of the central tryptic peptide ([M+2H]$^{2+}$ at *m/z* 917.36). The two Cys residues carry carbamidomethyl groups resulting from alkylation with iodoacetamide (+57.02 Da), together with −4.03 Da mass shifts. (*C*) UV/vis spectra of affinity-purified Buf1 and the Cys^{II}Ser+Cys^{III}Ser mutant. (*D*) NMR ROESY/TOCSY experiments to assign the resonances of the 19-mer peptide. (*E*) HNCACB experiment on the uniformly ^{13}C, ^{15}N-labeled peptide: sequential walk for the sequence following Cys^{II}. (*F*) The HNCO planes at the ^{15}N frequency of the indicated residues show classical ~175 ppm values for all carbonyl resonances, except for that downstream of a modified Cys, whose carbonyl carbon resonates at 184 ppm. (*G*) HNCO planes through the resonance of Lys24 that follows Cys^{II} while modifying the offset of the ^{13}C decoupling pulse during the C=O evolution period. Only when centered at 120 ppm is the 90-Hz carbon–carbon coupling refocused. (*H*) Measured NMR parameters and proposed structure for the Buf1 posttranslational modifications (shown for Cys^{II}).

modified, with a −10 Da mass shift (*SI Appendix*, Fig. S11). Similarly, Buf1 purified from a *C. vibrioides* culture induced with copper showed a −10 Da mass shift (*SI Appendix*, Fig. S12). To probe whether the modified Cys residues may be part of heterocycles as in other MNIO-modified RiPPs (7, 10), we recorded UV-visible absorption spectra of Buf1 and the Buf1$^{CysIISer+CysIIISer}$ variant. Consistent with the presence of aromatic heterocycles (30), the spectrum of the former showed a broad absorbance peak extending to 310 nm, unlike that of the latter (Fig. 3*C*). The spectrum of recombinant Buf2 similarly showed an absorbance maximum around 305 nm (*SI Appendix*, Fig. S13).

PTM Identification by NMR. To increase the yield of bufferin for structural elucidation by NMR, we coexpressed *bufA1* encoding an N-terminal His$_6$-SUMO-tag with *bufB1* and *bufC1* in *E. coli*. Purification of modified BufA1 followed by trypsin digestion and preparative HPLC allowed the preparation of the Cys^{II}- and Cys^{III}-containing 19-mer peptide at a milligram scale (*SI Appendix*, Fig. S14). Of note, this peptide was not cleaved by trypsin after Lys24 that immediately follows Cys^{II}, suggesting that the PTM on Cys^{II} somehow impacts the recognition of this Lys residue. The ^{1}H spectrum of the 19-mer peptide indicated two groups of anomalous resonances (*SI Appendix*, Fig. S15). By combining homonuclear ROESY and TOCSY experiments (31), they were assigned to the amide protons of Lys24 and Ala32 that follow the modified Cys^{II} and Cys^{III} residues, respectively, and to the Hα protons of Asp22 and Ser30 that precede them (Fig. 3*D*). Further analysis of these spectra showed the absence of both Hα and NH protons for the modified Cys residues. The absence of the latter was verified on a natural abundance ^{1}H, ^{15}N HSQC spectrum (*SI Appendix*, Fig. S15). These data suggest that their N and Cα atoms are part of heterocycles.

A ^{1}H, ^{13}C HSQC experiment showed correlations from the Asp22 and Ser30 Hα atoms to their own Cα carbons at 48.1 and 52.4 ppm, respectively, 6 ppm higher than their random coil values (32). The ^{1}H, ^{13}C HMBC spectrum connected the same Hα

protons to carbon atoms at 161.1 and 159.8 ppm, respectively (*SI Appendix*, Fig. S15). We produced a uniformly ^{13}C,^{15}N-labeled modified BufA1 molecule in *E. coli* and used its central tryptic peptide to obtain further carbon assignments on the basis of triple-resonance NMR experiments (33, 34). In the HNCACB experiment, we found no resonances that could correspond to upstream neighbors for Lys24 or Ala32, confirming that the Cα carbons of modified Cys^{II} and Cys^{III} do not resonate at the typical 50-ppm value expected for Cys residues (Fig. 3*E*). In a HNCO experiment starting from the amide groups of Lys24 or Ala32, we found values around 184 ppm for the C=O carbon atoms of both modified Cys residues (Fig. 3*F*), far from 175 and 200 ppm values expected for such atoms in random-coil and thio-amide peptides, respectively (35–38). By increasing the resolution and varying the offset of the decoupling pulse during the C=O evolution period, we determined a 90-Hz coupling constant of both carbonyls with carbon atoms whose chemical shift is ~120 ppm, consistent with their absence in the HNCACB experiment (Fig. 3*G*). Both parameters point to the C=O carbon atoms of the modified Cys residues connected to carbon atoms in aromatic rings (39).

Comparisons of the chemical shifts assigned on the modified BufA1 peptide with those found for a 5-thiooxazole-containing peptide (30) showed the same 6-ppm up-field shift of the Cα carbon of the preceding residue, the presence of similar carbon resonances at 120 and 160 ppm, and the 90-Hz coupling constant of the following carbonyl toward an aromatic ring carbon. Together with the MS data and the characteristic spectrophotometric spectrum (30), we conclude that the Buf1 modification implies cyclization of its central Cys residues to form thiooxazole groups (Fig. 3*H* and *SI Appendix*, Fig. S16).

Copper Binding by Bufferin 1. Since heterocycles can be involved in copper binding (40), we interrogated whether bufferins can complex with copper, which could be the basis for their protective effect. We first investigated complex formation in vivo by treating cultures of *buf1ABCD*-expressing bacteria with $CuSO_4$ prior to bufferin purification. Native MS analysis showed that purified Buf1 thus produced was fully loaded with copper, with a 1:1 stoichiometry (Fig. 4*A*). When *E. coli* producing $Buf1^{str}$ was exposed to a mixture of metals, native MS analysis of the purified peptide identified

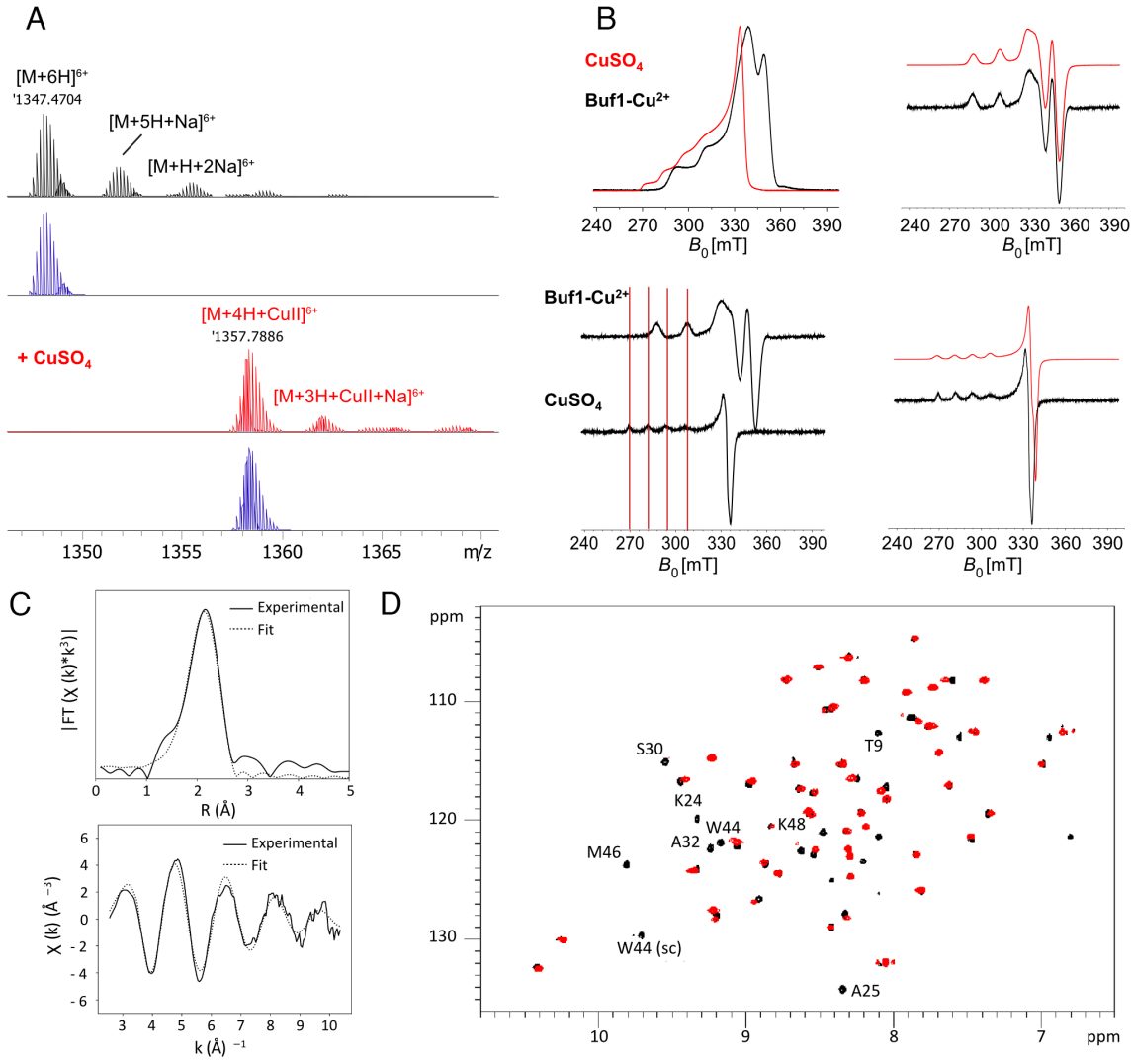

Fig. 4. Analyses of the bufferin 1-copper complex formed in vivo. (*A*) Native MS analysis of the purified complex: isotopic patterns of the major charge state (6+) species. The spectra in black and red show Buf1 from a nonsupplemented culture and from cultures supplemented with $CuSO_4$, respectively. The calculated isotopic patterns for $[M+6H]^{6+}$ and $[M+4H+CuII]^{6+}$ species are shown underneath. (*B*) Evidence for Cu^{2+} binding to Buf1 by EPR spectroscopy. Spectra of Echo-Detected Field-Swept of $CuSO_4$ (red) and of the Buf1–Cu^{2+} complex (black) are shown with the pseudo-modulation of the spectra underneath. The *Right* panels show the Easyspin fits (red) and the experimental spectra (black) for the Buf1–Cu^{2+} complex (*Top*) and for $CuSO_4$ (*Bottom*). (*C*) Experimental and fitted EXAFS spectra of the Buf1–Cu^{2+} complex (*Upper*) and corresponding Fourier transforms (*Lower*). (*D*) Superposition of the ^1H, ^{15}N HSQC spectra of apo Buf1 (black) and the Buf1–Cu^{2+} complex (red). sc = side chain.

the Buf1–Cu^{2+} complex, showing that the bufferin is selective for copper (*SI Appendix*, Fig. S17).

To gain insight into the mode of binding, we performed pulsed electron paramagnetic resonance (EPR) spectroscopy, X-ray absorption (XAS) spectroscopy, and NMR experiments. EPR spectra confirmed the stoichiometry and showed that Buf1 binds Cu^{2+}. The spectrum of the complex could be well reproduced by simulations involving 4 N atoms or 2 S and 2 N atoms in the first sphere of coordination of Cu^{2+} (41) (Fig. 4*B* and *SI Appendix*, Figs. S18 and S19 and Tables S2–S4). For the XAS experiments on the bufferin–Cu^{2+} complex (Fig. 4*C*), a good fit of the experimental data was obtained using a model with 2 N and 2 S atoms in the first coordination shell (*SI Appendix*, Table S5 and *SI Text*). By contrast, alternative models not including S atoms led to an unsatisfactory agreement between simulated and experimental data, leading us to discard the 4 N model.

To gain further insight into the binding site, we produced a ^{15}N,^{13}C-labeled Buf1 sample and recorded triple resonance spectra to assign its resonances. Simultaneously, we used the ^{1}H, ^{15}N HSQC plane as a basis for HSQC-NOESY and TOCSY experiments to confirm the assignments and gain some knowledge on structural aspects of Buf1. The sequential assignment was interrupted by the modified Cys residues, as expected. Amide resonances of the tryptic peptide and of the same segment in the full-length bufferin did not correspond at all, suggesting that the full-length sequence imposes structural constraints on the thiooxazole-containing loop. Part of these likely come from the β sheet spanning two short strands in the structural model, Thr9-Tyr13 and Trp44-Lys48 (*SI Appendix*, Fig. S1), that we confirmed experimentally through the strong Hα(i-1)–HN(i) NOE contacts between residues in these segments and the cross-strand NOE contacts between the amide protons of Lys45 and Cys12, and of Val47 and Glu10, respectively (*SI Appendix*, Fig. S20). Further analyses of the NOE spectrum also showed the characteristic amide i/i + 1 proton contacts that characterize the short predicted α helix (*SI Appendix*, Fig. S20). PTMs of the Cys^{II} and Cys^{III} residues hence do not interfere with the predicted 3D structure. We confirmed that Buf1 contains stable secondary structure by performing a Hydrogen/Deuterium exchange experiment. Labeled Buf1 was lyophilized from phosphate buffer and dissolved back in D_2O. After 1 h, a TOCSY spectrum showed remaining protons of the β strand (*SI Appendix*, Fig. S21). Amide protons of the first β strand comprising Cys12 hardly exchanged at all, whereas exchange was more pronounced for residues in the rest of the protein. This points to the β sheet as the major secondary structure element conferring stability to the bufferin.

A comparison of the spectra of Buf1 produced with or without copper showed many peaks unchanged, some experiencing a shift and a signal reduction, and yet others disappearing altogether (Fig. 4*D*). The latter most probably concern residues close to the paramagnetic Cu^{2+} ion. In particular, the disappearance of the peaks corresponding to direct neighbors of the heterocycles, such as Lys24, Ser30, and Ala32, supports the model that the thiooxazoles are involved in Cu^{2+} coordination. Interestingly, signals of Thr9, Trp44, Met46, and Lys48 predicted on the β-sheet face oriented toward the thiooxazole-containing loop also disappeared, indicating that residues of the β sheet may also contribute to the binding of copper.

Finally, we determined the binding affinities of Buf1 for Cu^{2+} and Cu^{+} by performing spectrophotometric competition assays as described (42). A K_D value of ~6×10^{-15} M was determined for the formation of a Buf1-Cu^{2+} complex (*SI Appendix*, Fig. S22). Using anaerobic conditions with Cu^{+}, we determined a K_D value of ~7×10^{-20} M for the Buf1-Cu^{+} complex. Buf1 can thus chelate both ions, with greater affinity for the more toxic Cu^{+} species (43).

BufB1 and BufC1 Are Required for Posttranslational Modification of Bufferin 1. To dissect the roles of individual *buf* genes, we constructed Cv_{buf1} derivatives that lack one or several genes and tested their growth phenotypes in the presence of $CuSO_4$. All deletion strains except for that lacking *bufD1* (*doxX*) displayed slow-growth phenotypes, showing that BufA1, BufB1, and BufC1, but not DoxX, are required for the function (Fig. 5*A*). LC-MS analysis confirmed that Buf1 is produced in the absence of the latter, indicating that DoxX is not necessary for installing PTMs (*SI Appendix*, Fig. S23).

To reveal the role of BufB1 and BufC1 in the bufferin maturation, we reconstituted the modification reaction in vitro using the purified proteins (*SI Appendix*, Fig. S24). Since MNIO enzymes require Fe^{II} and Fe^{III} ions for activity (9, 12), purified BufB1 was first analyzed by inductively coupled plasma–optical emission spectrometry, showing the presence of two Fe ions per BufB1 molecule. LC-MS analyses of the in vitro reactions showed that BufA1 was converted to a species with a −8 Da mass shift only when BufB1 and BufC1 were present (Fig. 5*B*). This mass shift corresponds to a species with two PTMs (−4 Da each) and lacking the S–S bond, due to the high concentration of reducing agent used in the in vitro assay. Indeed, trypsin digestion of thus modified BufA1 yielded the 19-residue peptide harboring two thiooxazole groups as confirmed by MS/MS analyses (Fig. 5*C*). Together with the gene inactivation data, these experiments established that BufB1 and BufC1 are required and sufficient to install the PTMs on BufA1.

The Sec Signal Peptide Is Dispensable for Heterocycle Formation. A notable feature of bufferin biosynthesis is that the precursor peptide harbors a predicted Sec signal peptide, which is rare in bacterial RiPP precursors. As shown by the MS data, the sequences of the bufferins are derived from cleavage of their BufA precursor at the predicted signal-peptidase cleavage site. To confirm the function of the BufA1's signal peptide, we fused it to leaderless β-lactamase (Bla), which becomes enzymatically active only after export to the periplasm. As a control, the first 7 residues of the BufA1 were also fused to Bla (*SI Appendix*, Fig. S25). *C. vibrioides* expressing the BufA1 signal peptide-Bla fusion displayed high levels of enzymatic activity in a spectrophotometric assay, unlike bacteria producing the control fusion, although both chimeric proteins were detected by immunoblotting (*SI Appendix*, Fig. S25).

To determine whether the signal peptide also acts as a leader peptide required for Cys transformation, we used the SUMO-*bufA1/bufB1/bufC1 E. coli* coexpression system. The *bufA1* gene was mutated to generate variant precursors with the signal peptide truncated eight residues from the N terminus [BufA1(-8 aa)] or completely removed [BufA1(CP)]. Subsequent LC-MS analysis of purified BufA1 after SUMO-tag cleavage indicated that both truncated precursors were still modified with a −10 Da shift, consistent with the presence of two thiooxazoles and one S–S bond (Fig. 5*D*). Thus, upon overexpression of the system without export of the bufferin, the Sec signal peptide is dispensable for PTMs, indicating that precursor recognition involves at least part of the core peptide. Nevertheless, this does not rule out the need for a leader sequence in natural conditions, which might partially overlap with the Sec signal peptide.

Discussion

Here, we report a bacterial strategy for copper homeostasis based on the synthesis of periplasmic RiPP metallophores. Incidentally, we also solved the conundrum of the gold-induced genes found in environmental and pathogenic bacteria (14–16). Bufferins form a RiPP family with original features and a specific function. We

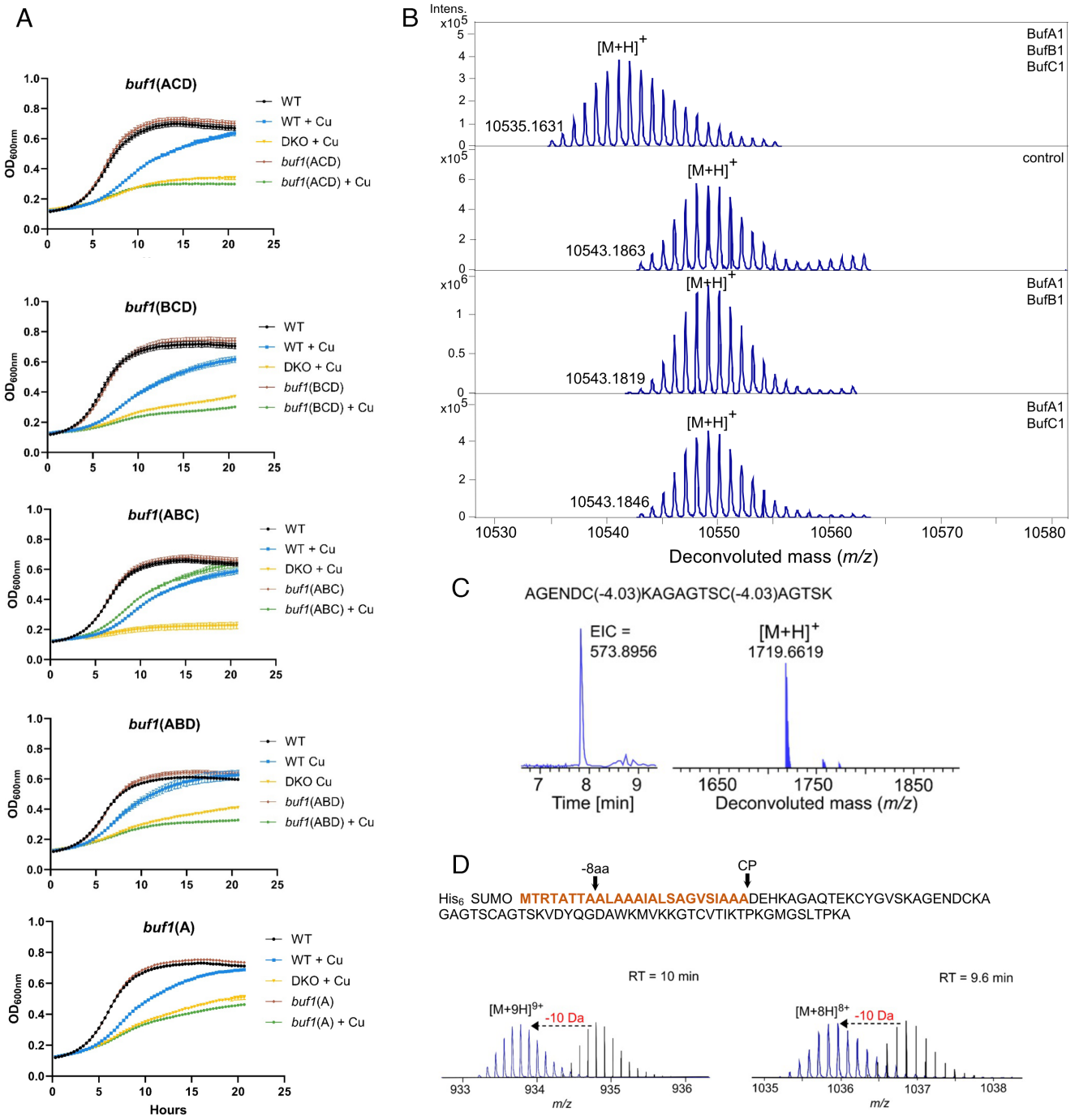

Fig. 5. Biosynthesis of bufferin 1. (*A*) Effect of Cu on the growth of *C. vibrioides* strains expressing the indicated genes. (*B*) In vitro reconstitution of Buf1 biosynthesis. The deconvoluted mass spectra for the products of the in vitro reactions are shown, with the added proteins indicated in the corresponding panels. Heat-denatured BufB1 and BufC1 were used for the control reaction. (*C*) LC-MS analysis of the 19-residue peptide of in vitro modified SUMO-Buf1. The extracted ion chromatogram (EIC) of $[M+3H]^{3+}$ (at *m/z* 573.8945) and the deconvoluted mass are shown. (*D*) Role of the signal peptide for the PTMs. A schematic representation of BufA1 variants with signal peptide truncations is shown on *Top*. LC-MS analyses of modified BufA1(-8 aa) (*Left*) and modified BufA1(CP) (*Right*): the MS spectra of the most abundant charge states $[M+9H]^{9+}$ and $[M+8H]^{8+}$, corresponding to deconvoluted monoisotopic masses $[M+H]^{+}$ of 8391.1281 and 8277.9398 (blue), respectively, are compared to the theoretical spectra of the unmodified peptides (black).

showed that they harbor a rare modification, 5-thiooxazole, installed by an MNIO enzyme. With thousands of homologs, bufferins are highly prevalent in bacteria and represent the largest family of MNIO-modified RiPPs.

The biosynthesis of bufferins involves unique features. To our knowledge, they are the first RiPPs known to exploit Sec signals for efficient translocation to the periplasm in the native producer. The presence of signal peptides in other RiPP precursors was previously suggested in cinnamycin (44) and recently reported for chryseobasin and oxazolin (7, 24), however, the latter were produced in heterologous hosts. Peptides with bulky modifications or macrocycles would be poor substrates of the Sec machinery due to the pore size of SecY (45). Although bufferins harbor an S–S bond formed macrocycle, it is most likely installed in the oxidizing periplasmic environment after export. This work establishes that the Sec and signal peptidase system represents a bona fide pathway for RiPP export and proteolytic maturation in bacteria.

The precursors and mature forms of bufferins are large compared to those of most RiPPs. Our structural analyses indicated that Buf1 contains stable secondary structure and is therefore a

small protein rather than a peptide. In addition, our in silico analyses identified larger bufferin-like precursors of more than 200 residues with numerous Cys residues and large predicted core sequences. Thus, the bufferin family appears to harbor a continuum ranging from modified peptides to bona fide proteins.

The conversion of Cys to 5-thiooxazole represents a previously unknown reaction catalyzed by MNIOs, further highlighting their chemical versatility. This rare PTM has been reported thus far only once in a natural product, catalyzed by a radical-SAM enzyme (30). Intense efforts have been made recently to explore the chemical space of MNIO-catalyzed transformations (7, 8, 11, 13, 46). In line with previous work on Cys-modifying MNIO enzymes, BufB would similarly make use of the mixed-valent iron center and proceed by an intermediate step of hydrogen atom abstraction from the Cβ of cysteine (9, 10, 12, 13) (*SI Appendix*, Fig. S26).

We demonstrated that model bufferins are involved in copper homeostasis by complexing with the metal. Notably, in vivo formation of the bufferin-Cu^{2+} complex most likely occurs while the unfolded bufferin emerges from the Sec machinery in the periplasm and folds around copper. This unique function for RiPPs contrasts with that of other MNIO-modified metallophores, methanobactins, a phylogenetically restricted family of RiPPs which essentially scavenge copper ions in the extracellular milieu for its provision to cuproprotein clients (47–50). The bufferin can bind both copper species, with greater affinity for the more toxic Cu^{+} ion, and copper binding involves the thiol groups of the thiooxazole cycles as well as N atoms. The defensive role of bufferins is reminiscent of those of nonribosomal peptides, anthrochelin, and yersiniabactin (51, 52). The putative multiple metal binding sites of large bufferins lead us to speculate that some of them might serve as intracellular metal reservoirs or contribute to transport of copper for disposal or storage. We believe that future studies on this large, diverse family might also unveil roles for bufferins in the homeostasis of other transition metals.

Copper is a major metal pollutant from anthropic sources (53, 54), and bufferins represent a previously unknown but highly prevalent mechanism of bacterial adaptation likely relevant in the environment, agriculture, and healthcare. In *C. vibrioides*, their expression is induced at rather high copper concentrations, suggesting that they come into play after other defense systems are overwhelmed. In *C. metallidurans*, the *gig/buf* operon was shown to be a minor system of protection, as the effect of its inactivation was felt only after other defense systems were also knocked out (20). Genetic determinants that provide environmental species with some protection against transition metals can contribute to the emergence of opportunistic pathogens (55), as exemplified by *L. pneumophila* which harbors up to six bufferin BGCs. Bufferins are most likely beneficial to bacteria in host–pathogen interactions notably in phagosomal compartments (28, 43, 56), which might account for their presence notably in *Bordetella pertussis, Neisseria gonorrheae, Haemophilus influenzae,* and *Pseudomonas aeruginosa*. From a more applied perspective, it should be possible in the long term to engineer bufferin variants for bioremediation purposes (3).

Materials and Methods

Genetic Constructs and Growth Conditions. Construction details, plasmids, recombinant strains, primers, and synthetic genes are described in *SI Appendix*, Tables S6–S8 and *SI Text*, respectively.

Functional Experiments. *C. vibrioides* growth curves were recorded using a TECAN Spark plate reader, with OD_{600} measurements every 20 min. Gain-of-function experiments were performed in *E. coli* expressing the *buf*1 operon under the control of an IPTG-inducible promoter or the lasso peptide pseudomycoidin operon from the same plasmid backbone (27). The bacteria were challenged with 0.3 mM $CuSO_4$ for 4 h in M9 medium (Cu^{2+} challenge), or with 2.7 mM $CuSO_4$ and 2 mM ascorbate in microaerobic conditions for 2 h in 2YT medium (Cu^{+} challenge). For the predation experiments, *Dictyostelium discoidum* was placed at the center of bacterial lawns before incubation at 20 °C for 3 d, and the densities of bacteria in the contact zones were determined with ImageJ. Experimental details are in *SI Appendix, SI Text*.

Bufferin Production and Purification. For Buf1 or Buf2 production in *C. vibrioides*, strains harboring the pSigF plasmid were grown overnight in PYE medium containing 100 μM IPTG, and the bufferins were purified on Streptactin or Ni-NTA columns using standard procedures. Production of isotopically labeled Buf1 was performed in *E. coli* BL21. For the in vitro assays, N-His_6-SUMO-BufA1, N-His_6-BufB1, and N-His_6-BufC1 were produced in BL21(DE3), purified on Ni-NTA columns, with 10 mM Tris(2-carboxyethyl)phosphine hydrochloride added to all buffers for BufA1. Production of the tryptic peptide for NMR studies was performed in BL21(DE3) coexpressing SUMO-BufA1, BufB1, and BufC1. The iron content of His_6-BufB1 was measured using an inductively coupled plasma–optical emission spectrometer (ICP-OES 5110 VDV, Agilent Technologies). Experimental details are provided in *SI Appendix, SI Text*.

Peptide Analyses by MS. All experimental details are given as *SI Appendix, SI Text*.

NMR Analyses. The central tryptic peptide was purified by preparative HPLC. All NMR spectra were recorded at 293 K on an 800-MHz NEO Bruker spectrometer equipped with a QCP cryogenic probe head. Experimental details are in *SI Appendix, SI Text*.

EPR Experiments. Pulsed EPR experiments were performed on the $Buf1^{twstr}$–copper complex using an ELEXSYS E-580 spectrometer (Bruker). Experimental details are in *SI Appendix, SI Text*. Numerical simulation of the spectra was conducted using the Matlab toolbox Easyspin 5.2.36.

XAS Experiments. XAS data on the $Buf1^{str}$–copper complex were acquired at the European Synchrotron Radiation Facility (ESRF). Details on the experiments and simulations are provided in *SI Appendix, SI Text*.

Spectrophotometric Copper Binding Assays. This was performed as described (42). Details are in *SI Appendix, SI Text*.

Enzymatic Assays In Vitro. Purified His-SUMO-BufA1 was digested with SUMO protease before adding either or both N-His_6-BufB1 and N-His_6-BufC1. After incubation, the mixtures were analyzed by LC-MSMS. β-lactamase assays were performed using spectrophotometry, with nitrocefin as a substrate. Details are presented as *SI Appendix, SI Text*.

In Silico Analyses. The search for putative bufferin precursors and the SSN analyses are detailed in *SI Appendix, SI Text*.

Data, Materials, and Software Availability. Raw data (MS, EPR, XAS) were deposited in Zenodo (57). All other data are included in the article and/or *SI Appendix*.

ACKNOWLEDGMENTS. We thank E. Lesne and G. Roy for initiating this work long ago, J.-M. Saliou for preliminary MS analyses, J.-Y. Matroule and P. Cherry for providing *C. vibrioides* strains, plasmids and protocols, and P. Faller for helpful discussions. This project was funded by the Agence Nationale de la Recherche (ANR) grant CuRiPP (ANR-22-CE44-0001-02) to F.J.-D. L. Leprevost and S. Jünger were supported by PhD fellowships of Lille University and of the French Ministry of Education (ED 227 MNHN-SU), respectively. S. Dubiley was supported by a fellowship of the Collège de France and by the Institut National de la Recherche pour l'agriculture, l'alimentation et l'environnement. We thank MetaboHub-MetaToul (Metabolomics and Fluxomics facilities, Toulouse, France (http://www.mth-metatoul.fr), part of the French National Infrastructure for Metabolomics and Fluxomics (http://www.metabohub.fr) funded by a grant from the Agence Nationale de la Recherche (MetaboHUB-ANR-11-INBS-0010) for access to NMR facility. The LC-MS data were acquired at the MNHN bioorganic mass spectrometry platform and the Plateforme d'analyse protéomique de Paris Sud Ouest (PAPPSO) platform (http://pappso.inra.fr/en). For the EPR experiments, the financial support from the IR INFRANALYTICS FR2054 is acknowledged. ICP-OES measurements were performed by V. Alaimo on the Chevreul Institute Platform (U-Lille/CNRS). The Region Hauts de France and the French government are acknowledged for funding this apparatus.

We thank the ESRF for provision of synchrotron radiation facilities under proposal number LS-3308 and Olivier Proux for assistance and support in using Beamline BM16 (FAME-UHD).

Author affiliations: [a]Univ. Lille, CNRS, INSERM, Centre Hospitalier Universitaire de Lille, Institut Pasteur de Lille, U1019 - UMR 9017 - Center for Infection and Immunity of Lille, Lille F-59000, France; [b]Unit Molecules of Communication and Adaptation of Microorganisms, UMR 7245 CNRS, Museum National d'Histoire Naturelle, Paris 75005, France; [c]Toulouse Biotechnology Institute, CNRS/Institut National de la Recherche en Agronomie, Alimentation et Environnement/Institut National des Sciences Appliquées, Toulouse 31077, France; [d]CNRS, UMR 8516 Laboratoire de Spectroscopie pour les Interactions, la Réactivité et l'Environnement, Université de Lille, Lille F-59000, France; [e]Institut National de la Recherche en Agronomie, Alimentation et Environnement-AgroParisTech-Université Paris-Saclay, Microbiologie des aliments au service de la santé, Jouy-en Josas 78352, France; [f]Laboratoire de Chimie de Coordination, CNRS UPR 8241, Toulouse 31077, France; and [g]Department of Physics, University of Rome Tor Vergata and Istituto Nazionale di Fisica Nucleare, Rome 00133, Italy

Author contributions: G.L., R.A., S.Z., S.D., Y.L., and F.J.-D. designed research; L.L., S.J., G.L., C.G., G.S., L.O., E.F., E.d.S., A.R.-M., G.B., F.S., C.H., R.A., S.Z., and S.D. performed research; L.L., S.J., G.L., C.G., G.S., L.O., E.F., E.d.S., A.R.-M., G.B., F.S., C.H., R.A., S.Z., S.D., Y.L., and F.J.-D. analyzed data; and L.L., S.J., G.L., G.S., F.S., S.Z., S.D., Y.L., and F.J.-D. wrote the paper.

1. P. G. Arnison *et al.*, Ribosomally synthesized and post-translationally modified peptide natural products: Overview and recommendations for a universal nomenclature. *Nat. Prod. Rep.* **30**, 108–160 (2013).
2. Y. Li, S. Rebuffat, The manifold roles of microbial ribosomal peptide-based natural products in physiology and ecology. *J. Biol. Chem.* **295**, 34–54 (2020).
3. M. Montalban-Lopez *et al.*, New developments in RiPP discovery, enzymology and engineering. *Nat. Prod. Rep.* **38**, 130–239 (2021).
4. B. J. Burkhart, G. A. Hudson, K. L. Dunbar, D. A. Mitchell, A prevalent peptide-binding domain guides ribosomal natural product biosynthesis. *Nat. Chem. Biol.* **11**, 564–570 (2015).
5. J. R. Chekan, C. Ongpipattanakul, S. K. Nair, Steric complementarity directs sequence promiscuous leader binding in RiPP biosynthesis. *Proc. Natl. Acad. Sci. U.S.A.* **116**, 24049–24055 (2019).
6. A. M. Kloosterman, K. E. Shelton, G. P. van Wezel, M. H. Medema, D. A. Mitchell, RRE-Finder: A genome-mining tool for class-independent RiPP discovery. *mSystems* **5**, e00267-20 (2020).
7. R. S. Ayikpoe, L. Zhu, J. Y. Chen, C. P. Ting, W. A. van der Donk, Macrocyclization and backbone rearrangement during RiPP biosynthesis by a SAM-dependent domain-of-unknown-function 692. *ACS Cent. Sci.* **9**, 1008–1018 (2023).
8. V. T. Chioti, K. A. Clark, J. G. Ganley, E. J. Han, M. R. Seyedsayamdost, N-Calpha bond cleavage catalyzed by a multinuclear iron oxygenase from a divergent methanobactin-like RiPP gene cluster. *J. Am. Chem. Soc.* **146**, 73132–77323 (2024).
9. C. Dou *et al.*, Crystal structure and catalytic mechanism of the MbnBC holoenzyme required for methanobactin biosynthesis. *Cell Res.* **32**, 302–314 (2022).
10. G. E. Kenney *et al.*, The biosynthesis of methanobactin. *Science* **359**, 1411–1416 (2018).
11. D. T. Nguyen *et al.*, Biosynthesis of macrocyclic peptides with C-terminal beta-amino-alpha-keto acid groups by three different metalloenzymes. *Acs Central Sci.* **10**, 1022–1032 (2024).
12. Y. J. Park *et al.*, A mixed-valent Fe(II)Fe(III) species converts cysteine to an oxazolone/thioamide pair in methanobactin biosynthesis. *Proc. Natl. Acad. Sci. U.S.A.* **119**, e2123566119 (2022).
13. C. P. Ting *et al.*, Use of a scaffold peptide in the biosynthesis of amino acid-derived natural products. *Science* **365**, 280–284 (2019).
14. K. Jwanowski *et al.*, The Legionella pneumophila GIG operon responds to gold and copper in planktonic and biofilm cultures. *PLoS One* **12**, e0174245 (2017).
15. C. Kohler, R. F. Lourenco, G. M. Avelar, S. L. Gomes, Extracytoplasmic function (ECF) sigma factor sigmaF is involved in Caulobacter crescentus response to heavy metal stress. *BMC Microbiol.* **12**, 210 (2012).
16. N. Wiesemann *et al.*, Influence of copper resistance determinants on gold transformation by Cupriavidus metallidurans strain CH34. *J. Bacteriol.* **195**, 2298–2308 (2013).
17. L. Maertens, P. Cherry, F. Tilquin, R. Van Houdt, J. Y. Matroule, Environmental conditions modulate the transcriptomic response of both Caulobacter crescentus morphotypes to Cu stress. *Microorganisms* **9**, 1116 (2021).
18. L. Coutte *et al.*, Combined RNAseq and ChIPseq analyses of the BvgA virulence regulator of Bordetella pertussis. *mSystems* **5**, e00208-20 (2020).
19. A. T. Tveit *et al.*, Widespread soil bacterium that oxidizes atmospheric methane. *Proc. Natl. Acad. Sci. U.S.A.* **116**, 8515–8524 (2019).
20. N. Hirth *et al.*, Full copper resistance in Cupriavidus metallidurans requires the interplay of many resistance systems. *Appl. Environ. Microbiol.* **89**, e0056723 (2023).
21. E. Severi, G. H. Thomas, Antibiotic export: Transporters involved in the final step of natural product production. *Microbiology (Reading)* **165**, 805–818 (2019).
22. F. H. Müller *et al.*, Coupling of the pathway of sulphur oxidation to dioxygen reduction: Characterization of a novel membrane-bound thiosulphate:quinone oxidoreductase. *Mol. Microbiol.* **53**, 1147–1160 (2004).
23. S. Nambi *et al.*, The oxidative stress network of Mycobacterium tuberculosis reveals coordination between radical detoxification systems. *Cell Host Microbe* **17**, 829–837 (2015).
24. O. M. Manley *et al.*, A multi-iron enzyme installs copper-binding oxazolone/thioamide pairs on a nontypeable Haemophilus influenzae virulence factor. *Proc. Natl. Acad. Sci. U.S.A.* **121**, e2408092121 (2024).
25. V. Waschulin *et al.*, Biosynthetic potential of uncultured Antarctic soil bacteria revealed through long-read metagenomic sequencing. *ISME J.* **16**, 101–111 (2022).
26. C. E. Alvarez-Martinez, R. L. Baldini, S. L. Gomes, A Caulobacter crescentus extracytoplasmic function sigma factor mediating the response to oxidative stress in stationary phase. *J. Bacteriol.* **188**, 1835–1846 (2006).
27. T. Zyubko *et al.*, Efficient in vivo synthesis of lasso peptide pseudomycoidin proceeds in the absence of both the leader and the leader peptidase. *Chem. Sci.* **10**, 9699–9707 (2019).
28. X. Hao *et al.*, A role for copper in protozoan grazing–Two billion years selecting for bacterial copper resistance. *Mol. Microbiol.* **102**, 628–641 (2016).
29. G. Prunier *et al.*, Fast alignment of mass spectra in large proteomics datasets, capturing dissimilarities arising from multiple complex modifications of peptides. *BMC Bioinformatics* **24**, 421 (2023).
30. J. K. Lewis *et al.*, New role for radical SAM enzymes in the biosynthesis of thio(seleno)oxazole RiPP natural products. *Biochemistry* **60**, 3347–3361 (2021).
31. K. Wüthrich, *NMR of Proteins and Nucleic Acids* (Wiley, New York, 1986).
32. D. S. Wishart, C. G. Bigam, A. Holm, R. S. Hodges, B. D. Sykes, 1H, 13C and 15N random coil NMR chemical shifts of the common amino acids. I. Investigations of nearest-neighbor effects. *J. Biomol. NMR* **5**, 67–81 (1995).
33. M. Sattler, Heteronuclear multidimensional NMR experiments for the structure determination of proteins in solution employing pulsed field gradients. *Progr. Nucl. Magn. Reson. Spectr.* **34**, 93–158 (1999).
34. T. Yamazaki, W. Lee, C. H. Arrowsmith, D. R. Muhandiram, L. E. Kay, A suite of triple resonance NMR experiments for the backbone assignment of 15N, 13C, 2H labeled proteins with high sensitivity. *J. Am. Chem. Soc.* **116**, 11655–11666 (1994).
35. D. S. Wishart, C. G. Bigam, A. Holm, R. S. Hodges, B. D. Sykes, (1)H, (13)C and (15)N random coil NMR chemical shifts of the common amino acids. I. Investigations of nearest-neighbor effects. *J. Biomol. NMR* **5**, 332 (1995).
36. K. E. Fiore *et al.*, Structural impact of thioamide incorporation into a beta-hairpin. *RSC Chem. Biol.* **3**, 582–591 (2022).
37. O. D. Hensens, G. Albers-Schönberg, Total structure of the peptide antibiotic components of thiopeptin by 1H and 13C. *J. Antibiot.* (Tokyo) **36**, 814–831 (1983).
38. H. O. Kalinowski, H. Kessler, Correlation of the 13C-NMR chemical shifts of carbonyl and thiocarbonyl groups. *Angew. Chem. Int. Ed. Engl.* **13**, 90–91 (1974).
39. V. Wray, Carbon-carbon coupling constants: A compilation of data and a practical guide. *Progr. Nucl. Magn. Reson. Spectr.* **13**, 177–256.
40. G. E. Kenney, A. C. Rosenzweig, Chalkophores. *Annu. Rev. Biochem.* **87**, 645–676 (2018).
41. B. Bennett, J. M. Kowalski, EPR methods for biological Cu(II): L-band CW and NARS. *Methods Enzymol.* **563**, 341–361 (2015).
42. L. Novoa-Aponte, C. Xu, F. C. Soncini, J. M. Arguello, The two-component system CopRS maintains subfemtomolar levels of free copper in the periplasm of Pseudomonas aeruginosa using a phosphatase-based mechanism. *mSphere* **5**, e01193-20 (2020).
43. K. S. Chaturvedi, J. P. Henderson, Pathogenic adaptations to host-derived antibacterial copper. *Front. Cell Infect. Microbiol.* **4**, 3 (2014).
44. D. A. Widdick *et al.*, Cloning and engineering of the cinnamycin biosynthetic gene cluster from Streptomyces cinnamoneus cinnamoneus DSM 40005. *Proc. Natl. Acad. Sci. U.S.A.* **100**, 4316–4321 (2003).
45. F. Bonardi *et al.*, Probing the SecYEG translocation pore size with preproteins conjugated with sizable rigid spherical molecules. *Proc. Natl. Acad. Sci. U.S.A.* **108**, 7775–7780 (2011).
46. K. A. Clark, M. R. Seyedsayamdost, Bioinformatic atlas of radical SAM enzyme-modified RiPP natural products reveals an isoleucine-tryptophan crosslink. *J. Am. Chem. Soc.* **144**, 17876–17888 (2022).
47. A. A. DiSpirito *et al.*, Methanobactin and the link between copper and bacterial methane oxidation. *Microbiol. Mol. Biol. Rev.* **80**, 387–409 (2016).
48. G. E. Kenney, A. C. Rosenzweig, Methanobactins: Maintaining copper homeostasis in methanotrophs and beyond. *J. Biol. Chem.* **293**, 4606–4615 (2018).
49. Y. Li *et al.*, Discovery and biosynthesis of tricyclic copper-binding ribosomal peptides containing histidine-to-butyrine crosslinks. *Nat. Commun.* **14**, 2944 (2023).
50. J. D. Semrau, A. A. DiSpirito, P. K. Obulisamy, C. S. Kang-Yun, Methanobactin from methanotrophs: Genetics, structure, function and potential applications. *FEMS Microbiol. Lett.* **367**, fnaa045 (2020).
51. H. Büttner, J. Hörl, J. Krabbe, C. Hertweck, Discovery and biosynthesis of anthrochelin, a growth-promoting metallophore of the human pathogen *Luteibacter anthropi*. *ChemBioChem* **24**, e202300322 (2023).
52. E. I. Koh, A. E. Robinson, N. Bandara, B. E. Rogers, J. P. Henderson, Copper import in Escherichia coli by the yersiniabactin metallophore system. *Nat. Chem. Biol.* **13**, 1016–1021 (2017).
53. B. M. Staehlin, J. G. Gibbons, A. Rokas, T. V. O'Halloran, J. C. Slot, Evolution of a heavy metal homeostasis/resistance island reflects increasing copper stress in enterobacteria. *Genome Biol. Evol* **8**, 811–826 (2016).
54. Z. Yu, L. Gunn, P. Wall, S. Fanning, Antimicrobial resistance and its association with tolerance to heavy metals in agriculture production. *Food Microbiol.* **64**, 23–32 (2017).
55. C. Baker-Austin, M. S. Wright, R. Stepanauskas, J. V. McArthur, Co-selection of antibiotic and metal resistance. *Trends Microbiol.* **14**, 176–182 (2006).
56. J. R. Sheldon, E. P. Skaar, Metals as phagocyte antimicrobial effectors. *Curr. Opin. Immunol.* **60**, 1–9 (2019).
57. L. Leprevost *et al.*, A widespread family of ribosomal peptide metallophores involved in bacterial adaptation to metal stress - (data). Zenodo. DOI: 10.5281/zenodo.14049532. Deposited 8 November 2024.